Effect of Geometrical Confinement on Ordering of Thermoplastic Polyurethanes With Crystallizable Hard and Soft Blocks

Ainur F. Abukaev , Marina Gorbunova , Denis V. Anokhin , Dimitri A. Ivanov *

Posted Date: 21 November 2023

doi: 10.20944/preprints202311.1240.v1

Keywords: thermoplastic polyurethane; poly(butylene adipate) diol; polycaprolactone diol; phase separation; crystallization kinetics; differential scanning calorimetry; infrared spectroscopy; X-ray diffraction

Article

Effect of Geometrical Confinement on Ordering of Thermoplastic Polyurethanes with Crystallizable Hard and Soft Blocks

Ainur F. Abukaev [1], Marina A. Gorbunova [1], Denis V. Anokhin [1] and Dimitri A. Ivanov [1,*]

Laboratory of Structural Methods of Materials Investigation, National University of Science and Technology MISIS, Leninskiy Prospekt 4, 119049 Moscow, Russia; mflute2008@yandex.ru (M.G.); anokhin@icp.ac.ru (D.A.); ainurabukaev@gmail.com (A.A.)

* Correspondence: dimitri.ivanov.2014@gmail.com

Abstract: The structural evolution and phase composition of multi-block thermoplastic polyurethanes, with different nature of the soft segments based on poly(butylene adipate) (PBA), were analyzed during in-situ thermal treatments. A combination of synchrotron small- and wide-angle X-ray scattering, differential scanning calorimetry, thermogravimetric analysis, and FTIR spectroscopy was used to determine the influence of macrodiol nature and crystallization conditions on the polymorphic behavior of PBA. Using a new synthesis scheme, a relatively high degree of crystallinity for urethane blocks was achieved, which depends on the diisocyanate type in the structure of the soft segment. The hard segment domains impose geometrical constraints on PBA, thereby altering its crystallization process compared to the neat oligomer. Thus, crystallization after annealing at a low temperature (80 °C) is fast, predominantly yielding a metastable β-phase. When heated to 180 °C, which is higher than the hard-segment melting temperature, a phase-separated structure is observed. Subsequent crystallization is slower, favoring the formation of the stable α-PBA modification. The phase separation can be observed even after the hard block melting. A notably slow crystallization from an isotropic melt was documented after the disruption of phase separation at 230 °C.

Keywords: thermoplastic polyurethane; poly(butylene adipate) diol; polycaprolactone diol; phase separation; crystallization kinetics; differential scanning calorimetry; infrared spectroscopy; X-ray diffraction

1. Introduction

Thermoplastic polyurethanes (TPU) belong to adaptive polymers due their response on external factors such as temperature [1,2], humidity [3], light [4] or pH [5,6]. They represent multi-block copolymers containing soft polyester (SS) and hard polyurethane (HS) segments. TPUs exhibit a shape memory effect, characterized by their ability to revert from a temporary form to a stable configuration. This phenomenon can be conceptualized within the framework of a double-network model, wherein the networks are systematically constituted by the domains of soft and hard blocks, respectively, as detailed in [7]. Switching of mechanical properties can be can be achieved through the melting of soft segment crystals. The transition temperature of a polyester is influenced by various factors including crystallization conditions, thermal history, and chemical composition, as evidenced in references [8–13]. Consequently, varying these parameters enables the control over the type and relative fraction of the crystalline phase, thereby facilitating the synthesis of materials with predetermined mechanical and thermodynamic properties.

Poly(butylene adipate) (PBA), a biodegradable polyester known for its rapid crystallization at room temperature (RT), ranks among the most prevalent materials in the fabrication of TPUs. This polymer is noted for its robust mechanical properties and is capable of forming two distinct polymorphic modifications: the thermodynamically stable monoclinic α-phase and the metastable

 doi:10.20944/preprints202311.1240.v1

orthorhombic β-phase, as documented in references [14,15].The α / β ratio in PBA-based polymers is defined by crystallization temperature [16], thermal history [17], epitaxy on ordered substrates [18] and mechanical stretching [19].

Typically, the formation of a metastable phase occurs under conditions far from equilibrium. When stored at RT, a phase transition from the β-phase to the α-phase is observed, characterized by the development of thick crystals, as indicated in reference [20]. Furthermore, the results of differential scanning calorimetry reveal complex thermal behavior dependent on the heating rate. This behavior is associated with the melting and recrystallization of the beta phase, followed by the melting of the alpha phase [21]. The presence of geometrical confinement, such as crystallization within anodic aluminum oxide templates featuring pore diameters of up to 100 nm, can also shift the equilibrium in favor of the beta phase.

As for the hard segments, aromatic 4,4'-diphenylmethane diisocyanate (MDI), and linear 1,6-hexamethylene diisocyanate (HMDI) linked with chain extender 1,4-butanediol (BD) are widely used in TPU synthesis [22–24]. Such hard segments in multi-block TPU form partially ordered mesophase stabilized by H-bonding [10]. The efficiency of the H-bonding is influenced by the chemical nature of the diisocyanates. Consequently, HMDI-BD, characterized by linear quasi-extended segments, forms a denser network compared to the aromatic MDI-BD, which impacts Young's modulus. The mutual influence on the ordering of SS and HS in TPUs can be attributed to the microphase separation of thermodynamically incompatible polyester and polyurethane blocks. The efficiency and rate of phase separation strongly depend on the nature and flexibility of the segments. For TPUs based on PCL and MDI variation of hard block composition results in formation of interconnected, isolated, and free domains of the hard blocks [25].

The influence of aliphatic (derived from HMDI) and cycloaliphatic (originating from IPDI) characteristics on the crystallization capabilities of polycaprolactone (PCL) blocks with varying molecular weights, as well as on the morphology of phase separation, was explored [26]. It was shown that a TPU based on IPDI exhibits a phase-compatible structure with one-phase transition above 0 °C, characterized by a single-phase transition above 0 °C. Additionally, the material demonstrates thermosensitive deformation at a temperature of 45 °C. In contrast, TPU based on HMDI exhibits superior shape memory properties, attributable to a phase-separated structure of melt-crystallized soft and hard blocks. Generally, the formation of small crystals, constrained by the size of nanodomains within a physical network, provides good mechanical strength and elastic properties. Since the crystallization of HS markedly enhances the phase separation of incompatible blocks, as noted in [27], it also occurs in an amorphous-amorphous state [28]. In our prior research [29,30], we investigated the crystal structure, supramolecular organization, and mechanical properties of TPUs based on PBA and PCL diols, focusing particularly on their evolution during extended storage periods. We emphasized the significance of physical aging and slow crystallization rate in influencing the behavior of these materials. Using ultra-fast calorimetry, we elucidated the influence of the HS composition and microphase separation on the crystallization kinetics and polymorphism of PBA in the diblock TPUs. Notably, effective phase separation of HMDI-based urethane and PBA facilitates the formation of a mesophase of HS and rapid crystallization of SS into the thermodynamically stable α-modification.

In the current paper, we investigate the structure formation of a novel series of multi-block TPUs incorporating hard and soft segments. The study employs a combination of small- and wide-angle X-ray scattering (SAXS/WAXS), differential scanning calorimetry (DSC), and Fourier transform infrared spectroscopy (FTIR), to examine ordering in these materials. We focus on elucidating the influence of phase separation within the TPU melt on the crystallization kinetics of both the HS and the SS, as well as on the phase composition of PBA.

 doi:10.20944/preprints202311.1240.v1

2. Materials and Methods

2.1. Materials

Poly(butylene adipate) diol (PBA) (Huakai Resin Co., Ltd., Shandong, China, and Merck, Darmstadt, Germany, Mn = 2000 Da) was dried in a vacuum at 80 °C for 4 hours. The hydroxyl group content, determined through a chemical method [32], was found to be 1.7 wt.%. 4,4'-Diphenylmethane diisocyanate (MDI) sourced from Alfa Aesar (Darmstadt, Germany) was utilized without further purification. 1,6-Hexamethylene diisocyanate (HMDI) from Merck (Darmstadt, Germany) underwent vacuum distillation at 50–55 °C/12 mm Hg and was subsequently stored in sealed ampoules. The chain extender, 1,4-butanediol (BD), also purchased from Merck (Darmstadt, Germany), was distilled over freshly powdered calcium hydride under reduced pressure. Dibutyltin dilaurate catalyst acquired from Merck (Darmstadt, Germany), was used as received.

2.2. Synthesis of Multi-Block Thermoplastic Polyurethane (TPU)

Multi-block TPUs were obtained through the stage of formation of macrodiiso-cyanate (MDC) in a solution of dichloromethane at RT in the presence of a catalyst from both the oligomer and macrodiols PBA, diisocyanates of aliphatic HMDI and aromatic MDI nature, as well as BD as a chain extender. Firstly, PBA macrodiols containing two PBA oligomers and a diisocyanate were obtained in two stages. At the first stage, a diisocyanate of an aliphatic (HMDI) or aromatic (MDI) nature was added to the PBA oligomer to obtain terminal NCO- groups, which then, at the second stage, reacted with the -OH groups of the PBA oligomer to produce PBA macrodiols of aliphatic and aromatic nature. Secondly, TPUs were synthesized by reaction of HMDI with PBA oligomer (TPU(PBA)) or with macrodiols based on HDMI (TPU(PBA-HMDI)) and MDI (TPU(PBA-MDI)) at [NCO]/[OH] ~ 2 to form MDC, then a chain extender was added BD and aromatic diisocyanate MDI to the stoichiometric ratio of functional groups ([NCO]MDI+HMDI/[OH] = 1). The mass fractions of reagent were the following: polydiol (69 %), diisocyanate (23 %) and chain extender (8 %). The SS/HS ratio was 2.2 for all samples. Polyurethane films were prepared from solution by drying at 40 °C for 24 hours. The mass fraction of the hard segment (based on HMDI, MDI and BD) was kept constant at 35%. Prior to conducting experiments, the native samples were stored at RT for two months.

Table 1. Chemical composition of studied TPUs.

N°	Sample	Polydiol	Diisocyanate	Chain Extender
1	TPU(PBA)	PBA	HMDI,MDI	BD
2	TPU(PBA-MDI)	PBA-MDI-PBA		
3	TPU(PBA-HMDI)	PBA-HMDI-PBA		

The hard segment content (HS, %) was calculated as follows:

$$\mathrm{HS}(\%) = \frac{(1+n)\,M(MDI+HMDI)+nM(\mathrm{BD})}{(1+n)\,M(MDI+HMDI)+nM(\mathrm{BD})+M(polydiol)}\mathrm{x}100\%$$

where *M(polydiol), M(MDI+HMDI)* and *M(BD)* are the molecular weights of PBA; diisocyanate and chain extender, respectively; n is the number of moles of BD. Chemical structure of synthesized TPUs is presented in Scheme 1.

Preprints (www.preprints.org) | NOT PEER-REVIEWED | Posted: 21 November 2023 doi:10.20944/preprints202311.1240.v1

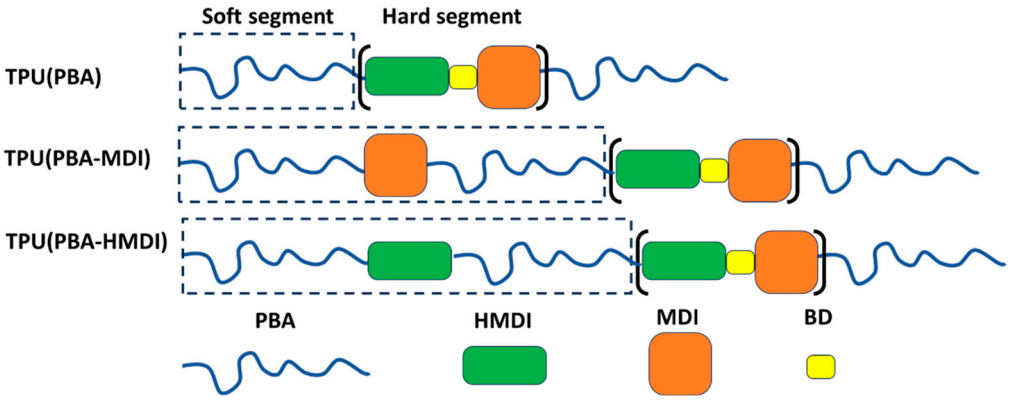

Scheme 1. Chemical structure of the synthesized TPUs.

2.3. Characterization

The thermal degradation behavior of the samples was investigated using a TGA/STDTA851e (Mettler-Toledo, Greifensee, Switzerland) thermogravimetric analyser (TGA). The analyses were conducted at a standard heating rate (10 °C/min) from room temperature to 550 °C under a nitrogen flow of 20 ml/min. The sample masses used were approximately 5 mg each.

Thermal behavior of the samples was investigated with a DSC 3+ (Mettler Toledo, Greifensee, Switzerland) differential scanning calorimeter using standard (10 °C/min) heating and cooling rates. Thermal programs for non-isothermal (left) and isothermal (right) crystallization were shown in Scheme 2. Multiple endothermic events were separated by fitting with several Gaussian peaks. The ΔHm (melting enthalpy) and T_{max} (maximum temperature) were determined as the area and maximum of the respective Gaussian peak. The onset temperature (T_{onset}) was defined as the point ща intersection between the tangent line at the half-width position and the baseline.

Duration of isothermal crystallization was 10 min for T_c. The degree of crystallinity (χc) was calculated from total melting enthalpy of PBA ($\Delta H°_m$ = 95 J/g) as reported in [33]:

$$\chi c = \frac{\Delta Hm}{\Delta H°m} \quad (1)$$

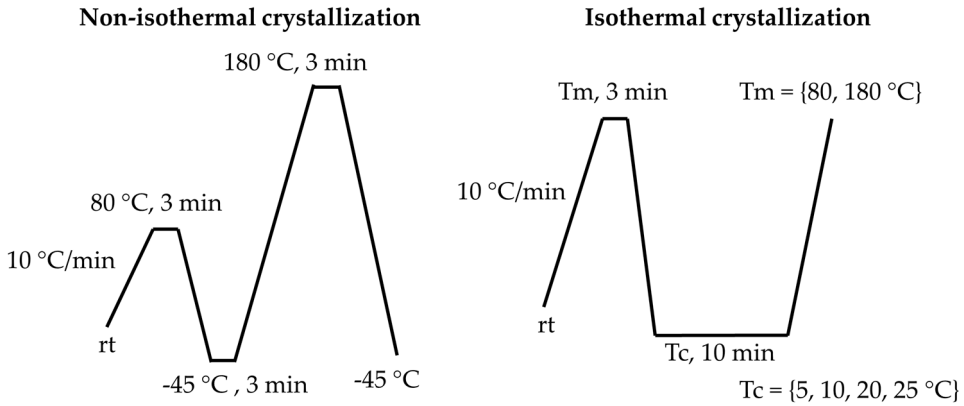

Scheme 2. DSC thermal programs for non-isothermal (left) and isothermal (right) crystallization.

The structure and phase composition of TPU at different temperatures was analyzed by the SAXS/WAXS technique at the BM26 beamline of the European Synchrotron Radiation Facility (ESRF) in Grenoble (France) using wavelength of 1.03Å. The X-ray scattering patterns were captured with 10-second exposures, utilizing two-dimensional Dectris Pilatus 1M and 300k detectors for SAXS and WAXS, respectively. Temperature control was provided by Linkam DSC600 heating stage. The modulus of the scattering vector s was calibrated using several diffraction orders of silver behenate.

 doi:10.20944/preprints202311.1240.v1

1D reduction of two-dimensional scattering patterns, background subtraction and curve fitting were carried out with a home-built software. The crystallinity index (χ_{WAXS}) was calculated as follows:

$$\chi_{WAXS} = \frac{\int I_{cr} * s^2 ds}{\int (I_{cr} + I_{amor}) * s^2 ds} \quad (2)$$

where I_{cr} and I_{amor} – are the total intensities of all crystalline reflections and the amorphous halo on 1D-reduced curves. The maximum of SAXS peaks was calculated on the Lorentz-corrected curves after performing background subtraction.

The chemical structure and hydrogen bonding were investigated by Fourier transform infrared (FTIR) spectroscopy with Bruker Alpha (Bruker Daltonics GmbH & Co.KG, Bremen, Germany) spectrometer using a multiple attenuated total reflection (ATR) module under the following conditions: measurement range 4000–500 cm^{-1}, measurement step 2 cm^{-1} and the number of scans per spectrum −56.

3. Results

3.1. Thermal analysis

Thermal stability of the synthesized TPUs were studied by the TGA technique (Figure S1), the corresponding degradation temperatures are shown in Table 2. The initial degradation stage was detected in the range of 287-297°C with 5% weight loss, which corresponds to the initial breakdown of urethane and ester bonds. The main degradation occurs in three stages: 358-361°C (T1) 395-495 °C (T2) and 450-470°C (T3), which may be associated with the degradation of C-C bonds in the bulky rigid blocks.

Table 2. Thermogravimetric analysis results.

Sample	T_{onset},°C	$T_{50\%}$,°C	T_{endset},°C	T_2,°C	T_2,°C	T_3,°C
TPU(PBA)	297	385	487	361	395	478
TPU(PBA-MDI)	283	385	494	358	495	470
TPU(PBA-HMDI)	296	380	488	361	409	450

The thermal transitions and crystal phase content was analyzed by DSC. In the first heating ramp to 80 °C, the native TPU samples (stored after synthesis for 2 months at RT) were brought above the melting temperature of SS (Table 3, Figure 1a). All the native samples exhibited similar endothermic melting peaks, with their onset approximately at 40-41°C, indicating the formation of a thermodynamically stable crystal phase of PBA. However, the chemical composition of the macrodiols influences the total degree of crystallinity. The inclusion of MDI and HMDI in SS raises the crystallinity index (χ) from 14% to 21% and 27%, respectively, due to the formation of a denser physical network of hydrogen bonds (Table 3).

During the first cooling from 80 °C to -45 °C, the DSC curves of all samples exhibit exothermic peaks corresponding to the SS crystallization with an onset at 10.6-12.7 °C (Table 3, Figure 1a). Interestingly, TPU(PBA) and TPU(PBA-HMDI) demonstrate a significant increase in the degree of crystallinity following recrystallization, likely due to enhanced phase separation at T_m. In contrast, the non-isothermal crystallization of TPU(PBA-MDI) results in a decrease of χ_{DSC} from 21 to 15%, revealing a lower crystallization rate of this sample across all temperature range.

The DSC traces of the second heating to 180°C reveal melting of HS in addition to endothermic peaks related to melting of SS (Table 3, Figure 1b). For TPU(PBA) and TPU(PBA-MDI) a broad endothermic peak with T_{onset} = 84 °C, T_{peak} = 93 °C and ΔH = - 8 J/g corresponds to melting of the MDI-rich domains. For TPU(PBA-HMDI) the melting peak of the HDMI domain is narrower and more intense (T_{onset} = 125 °C, T_{peak} = 148 °C and ΔH = - 15 J/g), indicating formation of regular crystalline regions of HS. The second cooling from 180°C displays crystallization of HS only for TPU(PBA-HMDI). As a result, the HMDI crystal phase fully recovers following melting. Consequently, the crystallization of the soft segments (SS) occurs within the same geometrical confinements of the physical network established by the hard segments (HS), as it does after cooling from 80 °C, as

Preprints (www.preprints.org) | NOT PEER-REVIEWED | Posted: 21 November 2023 doi:10.20944/preprints202311.1240.v1

indicated in Table 3. In contrast, the crystallization temperature and final degree of crystallinity of TPU(PBA) and TPU(PBA-MDI) significantly decreased during cooling from Tm = 180 °C. This can correspond to the situation of soft confinement of amorphous HS domains or to partial mixing of HS and SS at 180°C (Table 3, Figure 1b).

Table 3. Thermal properties of the TPU soft segment extracted from DSC measurements.

Sample	First Heating			First Cooling			Second Heating			Second Cooling		
	T_{onset}, °C	T_{maxc}, °C	χ_{DSC}, %	T_{onset}, °C	T_{maxc}, °C	χ_{DSC}, %	T_{onset}, °C	T_{maxc}, °C	χ_{DSC}, %	T_{onset}, °C	T_{maxc}, °C	χ_{DSC}, %
TPU-PBA	40.7	46.6	14	11.2	4.6	25	30.7	47.1	37	2.6	-4.9	18
TPU-PBA-MDI	41.0	45.5	21	10.6	2.6	15	24.8	46.1	28	-4.5	-13.4	11
TPU-PBA-HMDI	40.4	44.5	27	12.7	6.6	33	29.7	24.2	36	15.6	8.7	33

The details of the PBA crystal phase formation were explored during isothermal DSC experiments (Figure 1c,d). After heating to T_m=80°C and subsequent crystallization at T_c < 10°C all the samples demonstrate PBA melting peaks similar to those detected in non-isothermal crystallization experiments (Figure 1c). The increase of Tm to 180°C results in a decrease of crystallinity of TPU(PBA) and TPU(PBA-MDI) due to the disturbed phase separation discussed above. In turn, the DSC curve of TPU(PBA-HMDI) demonstrates double melting peak that can indicate formation of a mixture of the α- and β-polymorphs of PBA during crystallization of the TPU at $T_c \leq 10$°C. The interpretation of the multiple melting events correlated with polymorphic behavior of PBA [34]. The authors showed that the defect crystals of the monoclinic α-modification melt prior to the orthorhombic β-PBA. However, both phases can transform to the α-PBA with thicker crystals that melt at a higher temperature. The β-to-α phase transformation is dependent on the heating rate; however, at a rate of 10 °C/min, this transformation was not detected, as noted in reference [35].

For TPU(PBA) and TPU(PBA-MDI) crystallized at T_c = 10°C the critical role plays the highest previous annealing temperature (Figure 1c). After annealing at 80°C, both samples show relatively high indices of crystallinity χ_{DSC}, whereas formation of crystalline phase was not detected after cooling from 180°C. A more complex behavior was observed after crystallization of SS at Tc=25°C (Figure 1c). The crystallization rate of TPU(PBA) is very low and subsequent heating curves do not show any melting peaks of PBA. After annealing at 80°C, TPU(PBA-MDI) and TPU(PBA-HMDI) demonstrate similar double melting peaks corresponding to formation of two PBA polymorphs. In addition, a small endothermic peak with an onset slightly higher than the previous isothermal crystallization temperature was observed. It is likely to be related to the melting of small metastable crystals and cannot be identified as a particular PBA polymorph [36].

After annealing at 180 °C and isothermal crystallization at 25 °C, the melting behavior of TPU(PBA-HMDI) is similar to the one discussed above. However, for TPU(PBA-MDI) the SS crystal phase was not formed since the physical network of HS does not recover during cooling and subsequent annealing at 25 °C. Thus, TPU(PBA-MDI) demonstrates the most pronounced dependence of crystallization kinetics on the previous highest melt temperature. The polymorphic behavior of SS as a function of composition and geometrical confinement was further studied by in-situ temperature-resolved SAXS/WAXS.

Preprints (www.preprints.org) | NOT PEER-REVIEWED | Posted: 21 November 2023 doi:10.20944/preprints202311.1240.v1

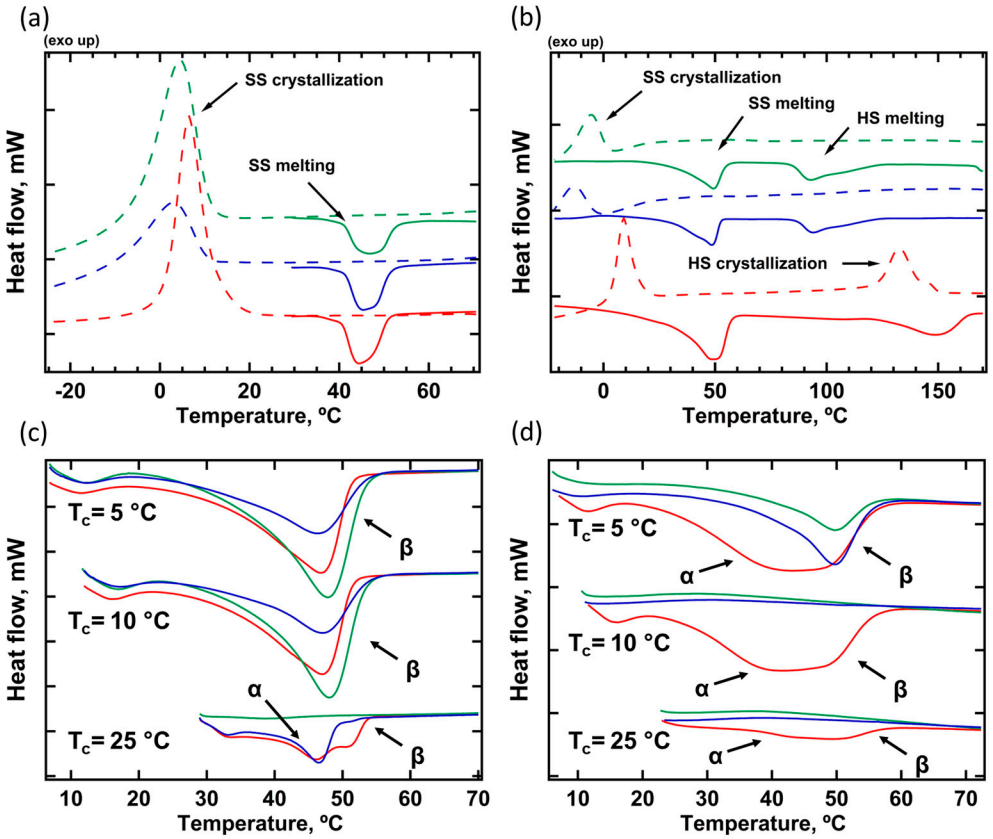

Figure 1. DSC curves TPU(PBA) (green), TPU(PBA-MDI) (blue) and TPU(PBA-HMDI) (red): (a) - first heating to 80°C (solid lines) and cooling to -45°C (dashed lines); (b) – second heating to 180°C (solid lines) and cooling to -45°C (dashed lines); (c) –heatings after cooling from 80°C and isothermal crystallization at Tc=5, 10 and 25°C; (d) – heatings after cooling from 180°C and isothermal crystallization at Tc=5, 10 and 25°C. The arrows indicate melting of the α- or β-polymorph of PBA.

3.2. Small- and wide-angle X-ray scattering

After long-term storage at RT, the WAXS diffractograms of all TPU samples exhibit the stable α-form of PBA and several additional reflections (Figure 2a). The latter are preserved after heating above the melting point of PBA and were attributed to the crystal phase of HS (Figure 2a). One can see that for TPU(PBA-HMDI) the crystals are formed by the HMDI blocks, while TPU(PBA) and TPU(PBA-MDI) exhibit MDI crystals [37,38]. The WAXS pattern of the HS based on HMDI consists of three peaks with d-spacings of 3.48, 3.97, 4.50 Å that point to the formation of two crystalline polymorphs observed in the DSC cooling curves. After crystallization at RT of the samples that were pre-heated to 80 and 180 °C, one can see the predominant formation of the metastable β-phase (Figure 2b). Interestingly, for TPU(PBA-HMDI) the pre-melting of the HS crystal phase at 180 °C shifts the α/β ratio to the more stable α-form of PBA due to slower crystallization rate at RT.

Preprints (www.preprints.org) | NOT PEER-REVIEWED | Posted: 21 November 2023 doi:10.20944/preprints202311.1240.v1

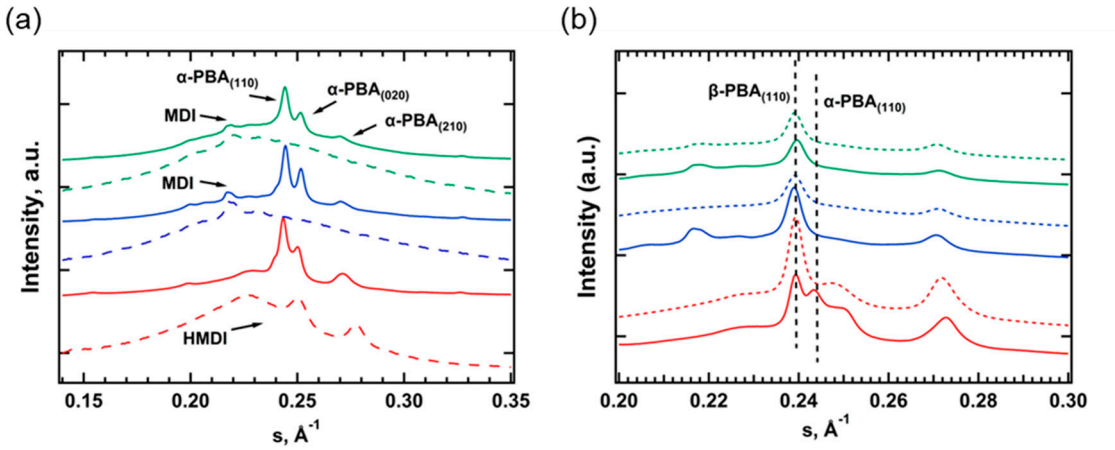

Figure 2. (a) – WAXS of TPU(PBA) (green), TPU(PBA-MDI) (blue), TPU(PBA-HMDI) (red): (a) native at RT (solid) and at 80 °C (dashed); (b) –at RT after cooling from 80 °C (solid) and 180 °C (dashed). Vertical lines indicate position of characteristic peaks of β and α-phase of PBA.

The analysis of crystallization kinetics of TPU at RT was performed with in-situ SAXS/WAXS by employing intense synchrotron radiation. The amount of the orthorhombic and monoclinic phases of PBA was estimated from the relative intensity of reflections at s=0.240 and 0.244 $Å^{-1}$, respectively (Figure 3a). One can see that the growth rate and relative fraction of each polymorph depend on the composition of HS and previous highest melt temperature (Figure 3b–d). The final crystallinity index and phase composition are shown in Table 4.

TPU(PBA) shows the lowest crystallization rates. Thus, upon 30 minutes crystallization at RT after cooling from 80 °C, the WAXS crystallinity index (χ_{WAXS}) reaches only 6.5 % with α/β=60/40. If before the experiment the sample was brought to 180 °C the crystallization of SS has not occurred even after 1 hour (Figure 3b). After annealing at 80 °C, the TPU(PBA-HMDI) sample based on highly crystalline HMDI crystallizes faster at RT, demonstrating a high fraction of β-PBA (Figure 3c). Upon melting of the HDMI block, the α-PBA forms more rapidly, but the total degree of crystallinity stays almost the same (Figure 3d). It is interesting to notice that HMDI crystallizes during cooling in the range 120 - 40 °C and its highest crystallinity is approximately 7%. For TPU(PBA-MDI), the MDI segment surrounded by PBA oligomers also crystallizes during cooling from 180 °C resulting in a twofold decrease of β-PBA fraction compared to cooling from 80 °C. In contrast, the crystallization kinetics of α-PBA is independent of the melt temperature, indicating that the nuclei of β-PBA are mainly formed from the phase-separated SS domains, whereas the α-nuclei are developed via β-to-α transition during crystallization. To understand the role of the phase separation of the blocks and geometrical confinement in crystallization of PBA, the SAXS patterns were analyzed.

Preprints (www.preprints.org) | NOT PEER-REVIEWED | Posted: 21 November 2023 doi:10.20944/preprints202311.1240.v1

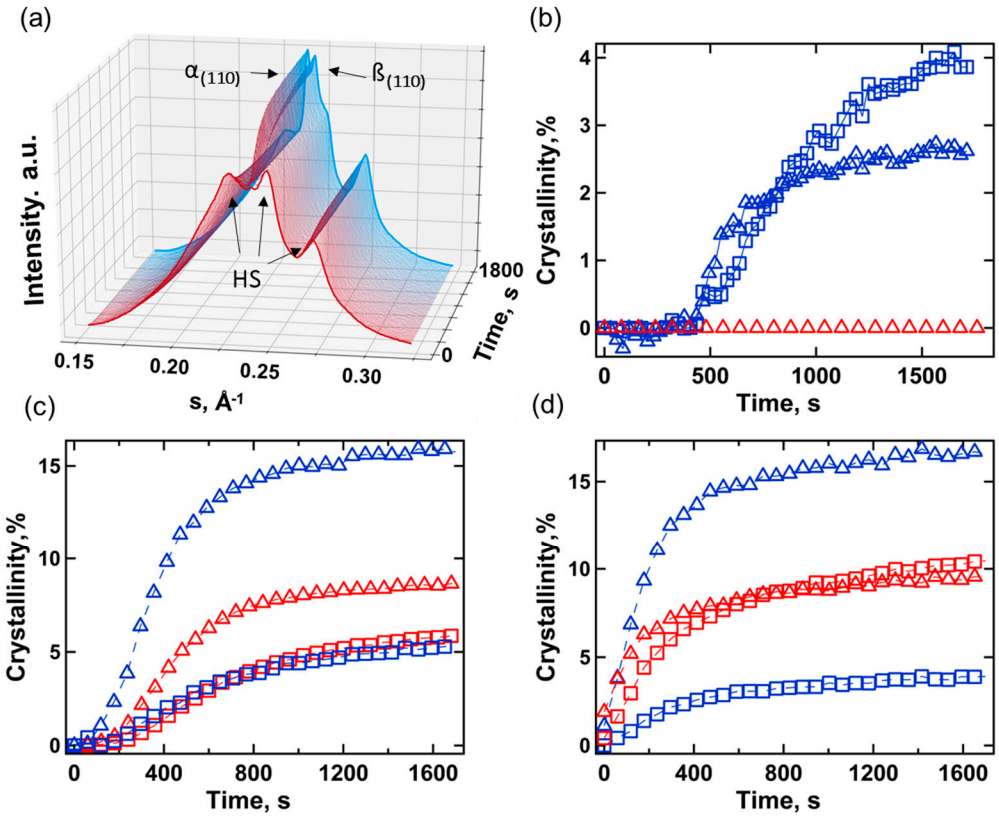

Figure 3. Evolution of WAXS diffractograms (TPU(PBA-HMDI)) during crystallization at RT after annealing at 80 °C (a); time dependence of the fractions of the α- (squares) and β (triangles) phase of PBA during crystallization at RT after annealing at 80°C (blue) and 180°C (red) of TPU(PBA) (b), TPU(PBA-MDI) (c), TPU(PBA-HMDI) (d).

Based on the SAXS peaks positions, the supramolecular structure can be described with three characteristic distances (Figure S2): the period between semi-crystalline SS and HS domains (L_1), the period between semicrystalline HS and molten SS (L_2) and the period between phase-separated amorphous HS and SS domains (L_3). The values of the small-angle maxima and their attribution (Figure S2) are given in Table 5.

For all samples, heating to 80 °C is paralleled by an increase of the long period by approximately 3 nm, attributable to the L1-L2 transition. This process is reversible upon cooling to RT. The TPU samples heated to 180 °C demonstrate a phase-separated morphology with large periodicity L_3, reaching up to 26.3 nm (Table 5). Upon returning to RT, TPU(PBA-HMDI) displays the formation of HMDI crystals with L2 = 15.2 nm immediately after cooling, followed by the crystallization of soft segments (SS) and the emergence of peak L1 = 14.3 nm. In the case of TPU(PBA), the SS does not crystallize after cooling, with its SAXS maximum located at 20.1 nm, possibly representing a superposition of L2 and L3 – a phase-separated morphology with limited crystallization of hard segments (HS). The situation is similar for TPU(PBA-MDI) immediately after cooling with the presence of L_2 and L_3 distances. However, after 30 minutes at RT, a shift of the SAXS maximum to wider angles is indicative of PBA crystallization.

Preprints (www.preprints.org) | NOT PEER-REVIEWED | Posted: 21 November 2023 doi:10.20944/preprints202311.1240.v1

Table 4. Crystallinity index and phase composition reached in the course of isothermal crystallization at RT.

Sample	Melt temperature, °C	χ_{WAXS}, %			FTIR
		total	α-PBA	ß-PBA	
TPU(PBA)	native	31	28	3	α
	80	7	4	3	α+β
	180		amorphous		amorphous
	230		amorphous		amorphous
TPU(PBA-MDI)	native	21	20	1	α
	80	21	5	16	α+β (>>β)
	180	15	6	9	α+β(>β)
	230		amorphous		amorphous
TPU(PBA-HMDI)	native	11	11	0	α
	80	21	4	17	α+β(>β)
	180	20	11	9	α+β
	230	10	5	5	α+β

Table 5. Results of SAXS analysis of TPU at different temperatures.

Temperature	SAXS distance, nm		
	TPU(PBA)	TPU(PBA-MDI)	TPU(PBA-HMDI)
25 °C	11.5 (L_1)	12.3 (L_1)	12.1 (L_1)
80 °C	14.6 (L_2)	15.6 (L_2)	15.2 (L_2)
25 °C 30 min after cooling from 80°C	12.6 (L_1)	13.1 (L_1)	12.4 (L_1)
180 °C	26.3 (L_3)	25.2 (L_3)	22.6 (L_3)
25 °C after cooling from 180 °C		21.3 (L_2 / L_3)	15.2 (L_2)
25 °C 30 min after cooling from 180°C	20.1 (L_2 / L_3)	16.1 (L_1 / L_2)	14.2 (L_1)

According to WAXS and SAXS, heating slightly above 230 °C, which is below the onset of decomposition, results in isotropization of TPU with formation of a mixed state of HS and SS . Cooling of TPU(PBA-HMDI) to RT demonstrates a behavior similar to cooling from the phase-separated state at 180 °C with the subsequent emergence of L_2 and L_1 distances (Figure 4). In contrast, for TPU(PBA) and TPU(PBA-MDI) samples, the crystal phases of SS and HS do not recover after cooling and remaining for 30 min at RT, with gradual development of the phase separated morphology (L_3 is 11 and 15 nm, respectively). After one week at RT, TPU(PBA) still demonstrates only an amorphous phase-separated state, whereas the PBA block of TPU(PBA-MDI) slowly crystallizes up to χ_{WAXS} = 4 %, with an absence of HS crystals (Figure S3).

Preprints (www.preprints.org) | NOT PEER-REVIEWED | Posted: 21 November 2023 doi:10.20944/preprints202311.1240.v1

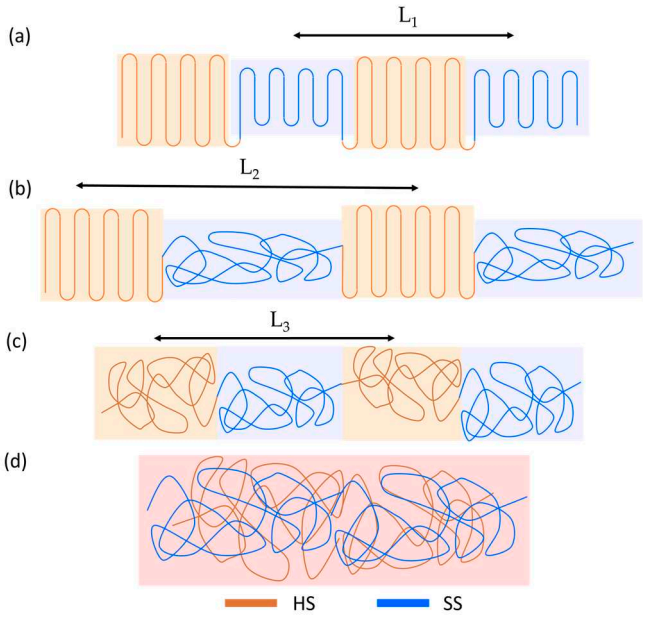

Figure 4. Schematic representation of the morphologies of the TPUs: HS crystal/SS crystal (a), structure after SS melting (b), amorphous phase-separated state (c) and amorphous isotropic state (d).

The complex interplay between the formation of a phase-separated morphology and crystallization of both types of segments can be illustrated on the example of the PBA-MDI sample (Figure 5). At RT, both segments are in the crystalline state (Figure 5a, red curve). On heating the sample to 80 °C, one observes melting of the SS accompanied by a shift of the SAXS peak position from 12.3 to 15.6 nm. This evolution corresponds to a change of the microstructure from the HS crystal/SS crystal state (Figure 4a) to the HS crystal/SS liquid state (Figure 4b), with a corresponding change of the characteristic SAXS distance from L1 to L2 (Figure 5b, black curve). At 180 °C, when the HS fully melts (Figure 5a,b, blue curves), the peak's intensity significantly decreases, while the characteristic SAXS distance increases to 25.2 nm. This situation corresponds to a structure with SS-liquid/HS-liquid phase separation (Figure 4c). Further increase of temperature to 230 °C leads to the isotropization of the melt, with disappearance of the SAXS signal pertinent to the phase-separated morphology (Figure 5b, blue curve). Upon cooling back to RT, the intensity of the SAXS signal increases again, indicating recovery of the phase-separated morphology (L3 = 15 nm). Notably, this occurs without any indications of crystallization (Figure 5a,b, orange curves). It is noteworthy that crystallization was not detected for both SS and HS even upon 30 min dwelling at RT.

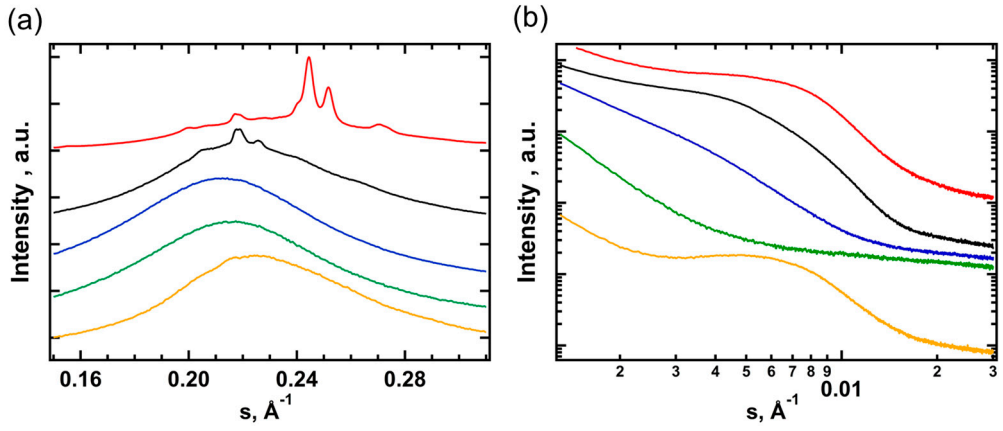

Figure 5. WAXS (a) and SAXS (b) curves for TPU(PBA-MDI) measured at RT (red), 80 °C (black), 180 °C (blue), 230 °C (green), and immediately after cooling from 230 °C to RT (orange).

Preprints (www.preprints.org) | NOT PEER-REVIEWED | Posted: 21 November 2023 doi:10.20944/preprints202311.1240.v1

These observations lead to the conclusion that the phase separation of SS and HS plays a critical role in the crystallization of the polyester, a finding corroborated by Fourier Transform Infrared (FTIR) spectroscopy measurements.

3.3. Study of morphology of TPUs with FTIR

The analysis of FTIR spectra of native samples, as well as those recrystallized after 80, 180 and 230 °C, reveals specific phase-separated morphology. The differences are observed in the region of absorption bands of amide (3500-3200 cm^{-1}) and carbonyl (1750-1650 cm^{-1}) groups (Figure 6).

For the native TPU(PBA) with the PBA oligomer as SS, the FTIR spectra display low-intensity bands of amide groups at 3393 and 3322 cm^{-1}, along with bands of carbonyl groups peaking at 1727 cm^{-1} and a shoulder spanning the range of 1700-1680 cm^{-1}, as seen in Figure 6a,d (blue curve). The presence of a minor low-intensity peak at 3443 cm^{-1}, corresponding to free amide groups of the urethane bond, as well as low-intensity peaks at 3322 and 3393 cm^{-1} and a shoulder in the 1700-1680 cm^{-1} region, suggests that most amide groups are in a weakly ordered state. The coexistence of these bands implies a relatively weak phase separation of blocks in amorphous regions. We hypothesize that this leads to increased polymer chain mobility and lower crystallinity compared to other samples. The recrystallization of the samples following annealing at 80 °C and 180 °C leads to an increase in H-bonding density. This change is manifested by the enhanced intensity of the bands corresponding to amide groups at 3500-3200 cm^{-1} and the band of H-bonded carbonyl groups of HS at 1700-1682 cm^{-1}, as depicted in Figure 6a,d (red and black curves). However, a reduction in the peak at 1726 cm^{-1} suggests a decrease in the number of dipole-dipole interactions in the crystal phase of PBA, likely due to slower crystallization (Figure 6a, black curves).

The incorporation of MDI into the PBA polymer chain (PBA-MDI) improves the phase-separated structure. This is evidenced by an increase in the shoulder of the H-bonded urethane segments at 1699 cm^{-1} for the native sample, as shown in Figure 6b (blue curve). This is further confirmed by the increase in the peak of hydrogen-bonded amide groups (3322 cm^{-1}). However, the peak at 3443 cm^{-1} is still observed (Figure 6e, black curve). Analogous to TPU(PBA), heating to temperatures of 80 °C and 180 °C improves the phase separation in TPU(PBA-MDI), as displayed in Figure 6b,e (red and black curves).

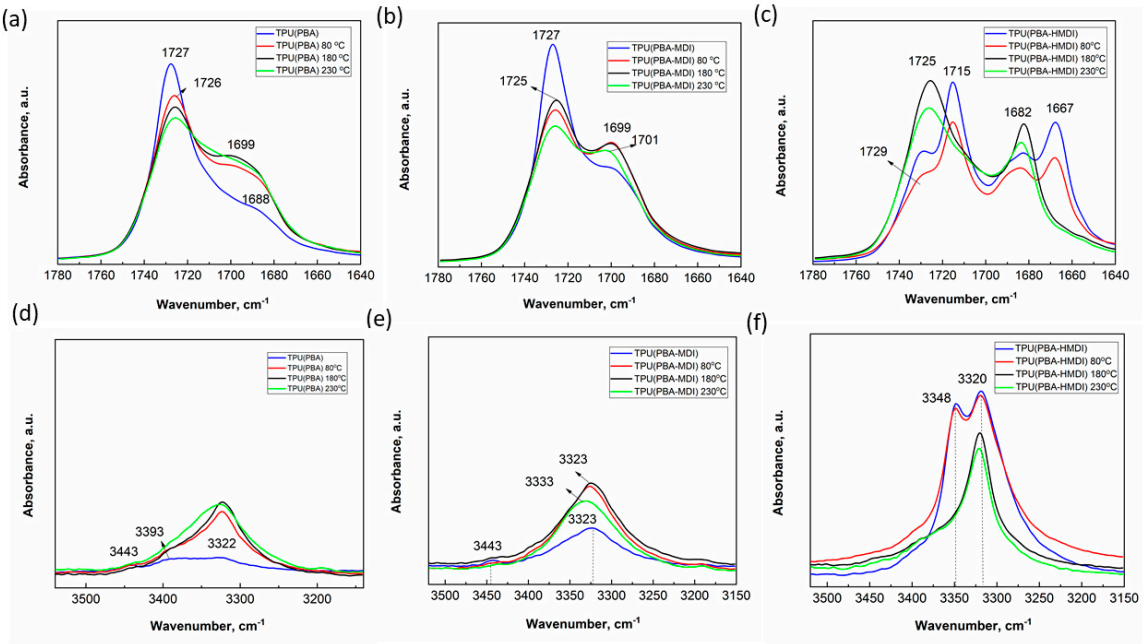

Figure 6. IR spectra in the absorption ranges 1780-1640 cm^{-1} (a-c) and 3500-3150 cm^{-1} (d-f) for the native samples and samples crystallized after heating to 80, 180 and 230 °C.

Distinct spectral patterns are observed for the TPU(PBA-HMDI) sample, which is based on a soft block of PBA with an aliphatic HMDI linker, as shown in Figure 6c,f. The native sample's spectrum exhibits pronounced peaks of C=O groups in the range of 1650-1683 cm^{-1} and N-H groups at 3322 and 3393 cm^{-1}, suggesting that HMDI forms an ordered network that effectively immobilizes the PBA chains (Figure 6c,f, blue curves). The increased number of peaks is associated with HMDI surrounded by PBA.

Crystallization following heating to 80 °C slightly disturbs the supramolecular structure (Figure 6c,f, red curves). However, heating to 180 °C destroys geometrical confinement of HS domains, significantly reducing the crystallization rate of PBA. The spectra of the sample after cooling to RT are similar to those of TPU(PBA) and TPU(PBA-MDI). However, there is a higher fraction of H-bonded carbonyl and urethane groups characteristic for phase separated morphology. This is attributed to the enhanced mobility of aliphatic diisocyanate (Figure 6c,f, black curves). The analysis of FTIR spectra reveals that integrating diisocyanate linkers into the polymer chain of the soft block increases the density of hydrogen bonding networks of urethane groups and leads to improved phase separation between the urethane groups of the soft and hard blocks, especially for samples where the soft block possesses an aliphatic nature.

FTIR spectra of TPU annealed at 230 °C corroborate the earlier TGA findings, demonstrating the chemical stability of the samples at this temperature (Figure S4). A certain decrease of intensity of the bands characterizing phase separation was found for all samples (Figure 6a-c, green curves). The second derivatives of the FTIR spectra in the region 1750-1650 cm^{-1} reveal a presence of a large fraction of mixed phase of SS and HS (Figure S5). The mixed phase can be responsible for the previously discussed decrease in the crystallization rate for TPU(PBA) and TPU(PBA-MDI). In general, the FTIR data are consistent with results obtained from DSC and WAXS/SAXS analyses. The chemical composition of the TPUs and their thermal history enable the regulation of the efficiency of phase separation and crystallization kinetics.

4. Conclusions

Thermoplastic polyurethanes with crystallizable hard and soft segments, based on aliphatic 1,6-hexamethylene diisocyanate and aromatic 4,4′-diphenylmethane diisocyanate and soft segments containing oligomer poly(butylene adipate) diol and its macrodiols of aliphatic and aromatic nature, were synthesized and characterized. The introduction of a diisocyanate segment between PBA blocks was observed to promote the crystallization of HS which, in turn, strongly affects crystallization of SS. Using a range of characterization techniques, including small- and wide-angle X-ray scattering, differential scanning calorimetry, thermogravimetric analysis, and FTIR spectroscopy, the study addressed the role of HS crystallites as geometrical confinement, influencing the efficiency of phase separation, crystallization kinetics, and the final phase composition of TPUs. Thermal analysis identified three characteristic temperatures responsible for ordering of the studied TPUs: the melting temperatures of the soft and hard segments, and the isotropization temperature. Accordingly, by heating to specific temperatures, one can stimulate the mobility of different segments and/or promote their crystallization. This enables the crystallization of PBA from isotropic, phase-separated, or geometrically confined states, which is crucial for determining the total crystallinity and polymorphic composition of the material.

TPU(PBA-HMDI) with HMDI linkers showed the highest crystallization rate and degree of crystallinity of SS, attributed to well-defined phase-separated domains stabilized by hydrogen bonding between linear urethane segments. The strong incompatibility between blocks enables rapid recovery of the phase-separated morphology following the melting of both SS and HS, and even after isotropization. This leads to fast crystallization of both HS and SS upon cooling, with crystallization of PBA favoring a large fraction of the metastable β-form. TPU(PBA-MDI) containing MDI bonded with PBA demonstrates lower crystallinity because of lower mobility of the aromatic diisocyanate. The slower crystallization of HS upon cooling does not provide formation of tight geometrical confinement, thereby reducing the rate of subsequent crystallization of PBA and favoring the formation of the more thermodynamically stable α-phase. TPU(PBA), which consists solely of PBA

oligomer in its SS, demonstrates slow crystallization of the polyester. The total crystallinity of this composition increases over several months, predominantly forming the α-modification. The melting of HS domains leads to a loss of phase separation and a consequent decrease in the crystallization rate of PBA. Isotropization at 230 °C totally suppresses crystallization of the sample due to low mobility of the segments in the mixed phase.

In situ studies of the crystallization kinetics have shown that TPU(PBA) exhibits the lowest rate of crystallization, yet it leads to the formation of a significant fraction of the stable α-polymorph. When the sample is heated above the melting temperature of the hard segment, the crystallization of PBA is completely suppressed. The crystallization rate of TPU(PBA-HMDI) is the highest and remains unaffected by the melt temperature. Owing to the rapid crystallization of the HMDI block upon cooling, this sample exhibits reduced sensitivity to the melting temperature and predominantly forms the metastable β-polymorph at room temperature. For TPU(PBA-MDI), the influence of geometrical confinement is most pronounced. In the presence of crystalline domains of hard segments, the soft segment demonstrates a high crystallization rate at room temperature, primarily leading to the formation of the β-phase of PBA. However, following the melting of MDI crystals at 180 °C, there is a significant decrease in the crystallization rate of PBA, resulting in the formation of the more stable α-phase of PBA.

The examination of FTIR spectra reveals that the introduction of diisocyanate linkers into the soft segment enhances the density of hydrogen bonding networks of urethane groups. This leads to more pronounced phase separation between the urethane groups of the soft and hard blocks, especially in samples with an aliphatic soft block.

Overall, our research underscores the significance of in situ analysis at each stage of ordering in designing thermoplastic polyurethanes with desired thermal and relaxation properties. These insights provide a more thorough understanding of the behavior of multi-block semi-crystalline TPUs with melting points near human body temperature, positioning them as promising candidates for the development of innovative medical materials.

Supplementary Materials: The following supporting information can be downloaded at the website of this paper posted on Preprints.org, Figure S1: TGA curves for the TPU samples measured at a rate of 10 °C/min in nitrogen atmosphere; Figure S2: SAXS curves of TPU(PBA-HMDI) (a, d), TPU(PBA) (b, e), TPU(PBA-MDI) (c,f): initial (red), after SS melting (black), at maximum temperature (blue), immediately after cooling (green) and after isothermal crystallization (yellow): Tm = 80 °C (a,b,c) and Tm = 180 °C (d,e,f); Figure S3: WAXS (a) and SAXS (b) curves for TPUs after cooling from 230°C and crystallization for 1 week at RT: TPU(PBA) (green), TPU(PBA-MDI) (blue), TPU(PBA-HMDI) (red); Figure S4: IR spectra for the native samples (black curve) and samples crystallized after heating to 230 °C (color curves); Figure S5: The second derivatives IR spectra TPU(PBA) (a), TPU(PBA-MDI) (b) and TPU(PBA-HMDI) (c) native samples (blue lines) and crystallized after 80°C (red lines), 180°C (black lines) and 230 °C (green lines).

Author Contributions: Conceptualization, M.G. and A.A.; Data curation, D.I., M.G.; Investigation, M.G., A.A; Formal analysis FTIR, M.G.; Formal analysis WAXS and DSC, A.A.; Methodology, M.G.; Supervision, D.A. and D.I.; writing—original draft preparation, A.A and M.G.; writing—review and editing, D.A. and D.I. All authors have read and agreed to the published version of the manuscript.

Funding: This research was funded by state support with the K1-2022-035 project in the frame of the strategic academic leadership program «Priority 2030».

Data Availability Statement: The data presented in this study are available in the article.

Acknowledgments: The authors acknowledge financial support from the National University of Science and Technology MISIS and state support with the K1-2022-035 project in the frame of the strategic academic leadership program «Priority 2030». The authors acknowledge the staff of the BM26 beamline at the European Synchrotron Radiation Facility (ESRF) in Grenoble (France) for their exceptional technical support.

Conflicts of Interest: The authors declare no conflicts of interest. The funders had no role in the design of the study; in the collection, analyses, or interpretation of data; in the writing of the manuscript, or in the decision to publish the results.

References

1. Lendlein, A.; Langer, R. Biodegradable, elastic shape-memory polymers forpotential biomedical applications. *Science* **2002**, 296 (5573), 1673–1676, doi: 10.1126/science.1066102.
2. Takahashi, T.; Hayashi, N.; Hayashi, S. Structure and properties of shape-memory polyurethane block copolymers. *J. Appl. Polym. Sci.* **1996**, 60, 1061, doi: 10.1002/(SICI)1097-4628(19960516)60:7<1061::AID-APP18>3.0.CO;2-3.
3. Wang, Y.; Cheng Z.; Liu, Z.; Kang, H.; Liu, Y. Cellulose nanofibers/polyurethane shape memory composites with fast water-responsivity. *J. Mater. Chem. B* **2018**, 6, 1668, doi: 10.1039/C7TB03069J.
4. Ji, S.; Fan, F.; Sun, C. ; Yu, Y.; Xu, H. Visible light-induced plasticity of shape memory polymers. *ACS Appl. Mater. Interfaces* **2017**, 9 (38), 33169–33175, doi: 10.1021/acsami.7b11188.
5. Lendlein, A.; Jiang, H.; Junger, O.; Langer, R. Light-induced shape-memory polymers, *Nature* **2005**, 434 (7035), 879–882, doi: 10.1038/nature03496.
6. Song, Q.; Chen, H.; Zhou, S.; Zhao, K.; Wang, B.; Hu, P. Thermo- and pH-sensitive shape memory polyurethane containing carboxyl groups. *Polym. Chem.* **2016**, 7 (9), 1739, doi: 10.1039/C5PY02010G.
7. Li, J.; Viveros, J.A.; Wrue, M.H.; Anthamatten, M. Shape-Memory Effects in Polymer Networks Containing Reversibly Associating Side-Groups. *Adv. Mater.* **2007**, 19, 2851, doi: 10.1002/adma.200602260.
8. Liu, W.; Zhang, R.; Huang, M.; Dong, X.; Xu, W.; Wang, Y.; Hu, G.H.; Zhu, J. Synthesis and shape memory property of segmented poly(ester urethane) with poly(butylene 1,4-cyclohexanedicarboxylate) as the soft segment. *RSC Adv.* **2016**, 6 (98), 95527–95534, doi: 10.1039/C6RA16325D.
9. Ahmad, M.; Xu, B.; Purnawali, H.; Fu, Y.; Huang, W.; Miraftab, M.; Luo J. High Performance Shape Memory Polyurethane Synthesized with High Molecular Weight Polyol as the Soft Segment. *Appl. Sci.* **2012**, 2, 535, doi: 10.3390/app2020535.
10. Yuan, X.; Sang, Z., Zhao, J.; Zhang, Z.; Zhang, J.; Cheng, J. Synthesis and properties of non-isocyanate aliphatic thermoplastic polyurethane elastomers with polycaprolactone soft segments. *J. Polym. Res.* **2017**, 24, 88, doi: 10.1007/s10965-017-1249-9.
11. Sabahi, N.; Roohani, I.; Wang C.H.; Farajzadeh, E.; Li, X. Thermoplastic polyurethane-based shape memory polymers with potential biomedical application: The effect of TPU soft-segment on shape memory effect and cytocompatibility. *Polymer* **2023**, 283, 121689., doi: 10.1016/j.polymer.2023.126189.
12. Wang, H.; Zhang, L.; Peh, P.; et al. Effect of Phase Separation and Crystallization on Enthalpy Relaxation in Thermoplastic Polyurethane. *Macromolecules* **2022**, 55, 19, 8566 – 8576, doi: 10.1021/acs.macromol.2c01504.
13. Frick, A.; Rochman, A.; Characterization of TPU-elastomers by thermal analysis (DSC). *Polymer Testing* **2004**, 23, 4, 413-417, doi: 10.1016/j.polymertesting.2003.09.013.
14. Minke, R.; Blackwell, J., Polymorphic Structures of Poly(tetramet hylene Adipate). *J. Macromol. Sci.-Phys., B* **1979**, 16(3), 407-417, doi: 10.1080/00222347908212305.
15. Zheng, Y.; Pan, P., Crystallization of biodegradable and biobased polyesters: Polymorphism, cocrystallization, and structure-property relationship. *Progress in Polymer Science* **2020**, 109, 101291, doi: 10.1016/j.progpolymsci.2020.101291.
16. Lotz, B.; Miyoshi, T.; Cheng, S. 50th anniversary perspective: polymer crystals and crystallization: personal journeys in a challenging research field. *Macromolecules* **2017**, 50, 5995–6025, doi: 10.1021/acs.macromol.7b00907.
17. Prasannan, A.; Bichtram, T.; et al. Nucleation effects of α-cyclodextrin inclusion complexes on the crystallization behavior of biodegradable poly(1,4-butylene adipate). *Cryst. Eng. Comm.* **2013**, 15, 5119, doi: 10.1039/c3ce26844f.
18. Wang, H.; Gao, Z.; Yang, X.; Liu, K.; Zhang, M.; Qiang, X.; Wang, X. Epitaxial Crystallization Behavior of Poly(butylene adipate) on Orientated Poly(butylene succinate) Substrate. *Polymer (Basel)* **2018**, 10(2), 110, doi: 10.3390/polym10020110.
19. Song, Y.; Ye, H.; Xu, J.; Hou, K.; Zhou, Q.; Lu, G. Stretch-induced bidirectional polymorphic transformation of crystals in poly(butylene adipate). *Polymer* **2014**, 55, 3054, doi: 10.1016/j.polymer.2014.05.011.
20. Bothe, M.; Emmerling, F.; Pretsch, T.; Poly(ester urethane) with Vary-ing Polyester Chain Length: Polymorphism and Shape-Memory Behavior. *Macromolecular Chemistry and Physics* **2013**, 214 (23), 2683-2693, doi: 10.1002/macp.201300464.
21. Sun, X.; Fang, Q.; Li, H.; Ren, Z.; Yan, S. Effect of Anodic Alumina Oxide Pore Diameter on the Crystallization of Poly(butylene adipate). *Langmuir* **2016**, 32(13), 3269-3275, doi: 10.1021/acs.langmuir.6b00251.
22. Chan-Chan, L.; Chan-Chan , L.; Solis-Correa, R.; Vargas-Coronado, R.; Cervantes-U, J.; Cauich-Rodríguez, J.; Quintana, P.; Bartolo-Pérez, P. Degradation studies on segmented polyurethanes prepared with HMDI, PCL and different chain extenders. *Acta Biomaterialia* **2010**, 6(6), 2035-2044, doi: 10.1016/j.actbio.2009.12.010.
23. Pielichowski, K.; Słotwińska, D.; Dziwiński, E.; Segmented MDI/HMDI-based polyurethanes with lowered flammability. *Journal of Applied Polymer Science*, **2004** 91(5), 3214-3224, doi: 10.1002/app.13519.

24. Herrera, M.; Matuschek, G.; Kettrup, A. Thermal degradation of thermoplastic polyurethane elastomers (TPU) based on MDI. *Polymer Degradation and Stability* **2002**, 78(2), 323-331, doi: 10.1016/S0141-3910(02)00181-7.
25. Ji F.; Hu, J.; Li, T.; Wong, Y. Morphology and shape memory effect of segmented polyurethanes. Part I: With crystalline reversible phase. *Polymer (Guildf)* **2007**, 48(17), 5133–5145, doi: 10.1016/j.polymer.2007.06.032.
26. Wang, Y.; Wang, L.; Liu, H.; He, S.; Lui, X.; Li, W.; Huang, M.; Chen, Z. Polyurethane as smart biocoatings: Effects of hard segments on phase structures and properties. *Prog. Org. Coatings.* **2021**, 150, 106000, doi: 10.1016/j.porgcoat.2020.106000.
27. Quiram, D.J.; Register, R.A.; Marchand, G.R.; Adamson, D.H. Chain Orientation in Block Copolymers Exhibiting Cylindrically Confined Crystallization. *Macromolecules* **1998**, 31, 4891–4898, doi: 10.1021/ma971218h.
28. Li, Y. J.; Ren, Z. Y.; Zhao, M.; Yang, H.C.; Chu, B.; Multiphase structure of segmented polyurethanes – effects of hard-segment flexibility. **Macromolecules 1993**, 26, 612–622, doi: 10.1021/ma00056a010.
29. Gorbunova, M.; Anokhin, D.V.; Abukaev, A.; Ivanov, D. The Influence of Long-Time Storage on the Structure and Properties of Multi-Block Thermoplastic Polyurethanes Based on Poly(butylene adipate) Diol and Polycaprolactone Diol. *Materials* **2023**, 16, 818, doi: 10.3390/ma16020818.
30. Gorbunova, M.A.; Anokhin, D.V.; Abukaev, A.F.; Ivanov, D.A. Impact of Soft Segment Composition on Phase Separation and Crystallization of Multi-Block Thermoplastic Polyurethanes Based on Poly(butylene adipate) Diol and Polycaprolactone Diol. *Crystals* **2023**, 13, 1447, doi: 10.3390/cryst13101447.
31. Gorbunova, M.A.; Komov, E.V.; Grunin, L.Yu.; Ivanova, M.S.; Abukaev, A.F.; Imamutdinova, A.M.; Ivanov, D.A.; Anokhin, D.V. Effect of separation of blocks on crystallization kinetics and phase composition of poly(butylene adipate) in multi-block thermoplastic polyurethanes. *Phys. Chem. Chem. Phys.* **2022**, 24, 902-913, doi: 10.1039/D1CP04684E.
32. Tarasov, A.E.; Lodygina, V.P.; Komratova, V.V.; Gorbunova, M.A.; Badamshina, E.R. New IR-Spectroscopic Methods for Determining the Hydroxyl Content in Oligomers. J. Appl. Spectrosc. **2017**, 84, 211–216, doi: 10.1007/s10812-017-0453-z.
33. He, Y.; Xie, D.; Zhang, X. The Structure, Microphase-Separated Morphology, and Property of Polyurethanes and Polyureas. *J. Mater. Sci.* **2014**, 49, 7339–7352, doi:10.1007/s10853-014-8458-y.
34. Gan, Z.; Kuwabara, K.; Abe, H.; Iwata, H.; Doi, Y. Metastability and Transformation of Polymorphic Crystals in Biodegradable Poly(butylene adipate). *Biomacromolecules* **2004**, 5, 371-378, doi: 10.1021/bm0343850.
35. Gan, Z.; Abe, H.; Doi, Y. Temperature-Induced Polymorphic Crystals of Poly(butylene adipate). *Macromol. Chem. Phys.* **2002**, 203(16), 2369-2374, doi: 10.1002/macp.200290007.
36. Mukhametzyanov, T.; Schmelzer, J.; Yarko, E.; Abdullin, A.; Ziganshin, M.; Sedov, I.; Schick, C. Crystal Nucleation and Growth in Cross-Linked Poly(ε-caprolactone) (PCL). *Polymers* **2021**, 13(21), 3617, doi: 10.3390/polym13213617.
37. D'hollander, S.; Gommes, C.J.; Mens,R.; Adriaensens, P.; Goderis, B.; Prez, F.D. Modeling the morphology and mechanical behavior of shape memory polyurethanes based on solid-state NMR and synchrotron SAXS/WAXD. *J. Mater. Chem.* **2010**, 20, 3475-3486, doi: 10.1039/B923734H.
38. Koberstein, J.T.; Galambos, A.F. Multiple Melting in Segmented Polyurethane Block Copolymers. *Macromolecules* **1992**, 25(21), 5618-5624, doi: 10.1021/ma00047a010.